

A Unified Weight Learning and Low-Rank Regression Model for Robust Face Recognition

Miaohua Zhang*, Yongsheng Gao*, Fanhua Shang[†]

* School of Engineering and Built Environment, Griffith University, Australia;

[†]School of Artificial Intelligence, Xidian University, China

lena.zhang@griffithuni.edu.au; yongsheng.gao@griffith.edu.au; fhshang@xidian.edu.cn

Abstract

Regression-based error modelling has been extensively studied for face recognition in recent years. The most important problem in regression-based error model is fitting the complex representation error caused by various corruptions and environment changes. However, existing works are not robust enough to model the complex corrupted errors. In this paper, we address this problem by a unified sparse weight learning and low-rank approximation regression model and applied it to the robust face recognition in the presence of varying types and levels of corruptions, such as random pixel corruptions and block occlusions, or disguise. The proposed model enables the random noise and contiguous occlusions to be addressed simultaneously. For the random noise, we proposed a generalized correntropy (GC) function to match the error distribution. For the structured error caused by occlusion or disguise, we proposed a GC function based rank approximation to measure the rank of error matrix. An effective iterative optimization is developed to solve the optimal weight learning and low-rank approximation. Extensive experimental results on three public face databases show that the proposed model can fit the error distribution and structure very well, thus obtain better recognition accuracy in comparison with the existing methods.

Introduction

The regression-based error model can be roughly classified into two categories: the mean square error (MSE) based ones and the robust function based ones. The most representative approaches of MSE-based approaches is the sparse representation classifier (SRC) (Wright et al. 2009) which takes advantages of the powerful feature selection ability of sparse representation to learn discriminative features for robust face recognition. Then, (Deng, Hu, and Guo 2017) extended the SRC by proposing an auxiliary intra-class variant dictionary to characterise the variation between the training and testing images. (Huang et al. 2013) took advantage of the $l_{2,1}$ -norm and took the label information into consideration to obtain more discriminative features. However, performances of these MSE-based methods mentioned above can be significantly deteriorated when the data are corrupted by outliers, which is inevitable in real-world applications. Outliers are typically far away from the centre of the normal

data, but MSE-based loss function assigns same weights to all measures without any discriminative constraints on ever severely or slightly corrupted ones when minimizing the representation error, as a consequence, such an equal weight assignment will result in an incorrect sparse solution. Moreover, the MSE-based loss function assumes that the error follows the Gaussian distribution, which is not only sensitive to non-Gaussian noise but also to outliers. As a consequence, these existing methods fail to approximate the sparse coding if the assumption does not hold (He, Zheng, and Hu 2011; Wang, Tang, and Li 2016; Chen et al. 2016). To overcome these drawbacks, (Wright et al. 2009) proposed a robust version of SRC to assume that the noise follow a Laplacian distribution. Then in order to handle illumination variations and strong noise, (Naseem, Togneri, and Bennamoun 2012) applied the Huber and Laplacian descriptor. (He, Zheng, and Hu 2011) proposed the CESR algorithm by using a correntropy induced metric to model the representation error. (Yang et al. 2012) proposed a regularized robust classifier (RRC) using the local quadratic approximation and a reweighted least squares solution is provided. (Zheng et al. 2017) proposed an iteratively reconstrained group sparse classifier (IRGSC) in which an adaptive weight learning procedure is proposed to give more emphasis on normal image pixels while suppressing the noise and outliers.

However, the above algorithms are based on the vector space and ignore the spatial correlation among error pixels, which cannot preserve the inherent structure of the image, resulting in inferior recognition performance. Recently, many researchers argue that the representation error has a specific structure when there are contiguous errors caused by partial occlusion (Iliadis et al. 2017; Xie et al. 2017; Yang et al. 2016). To make better use of the structure of error, (Qian et al. 2015) proposed to use the low-rank property to approximate the structure of the error image with occlusions. However, the rank minimization is an NP-hard problem and is difficult to be optimized. A convex-relaxation, i.e. nuclear norm, based regression (Yang et al. 2016) was proposed to approximate the rank of the error image. Although the nuclear norm based approximation has improved the performance of face recognition in the presence of occlusions. The nuclear norm based rank approximation treats each singular value equally, i.e. it shrinks each singular value with the same threshold regardless of their contribution to

the image reconstruction, which will lead to biased estimation. In face recognition problem, the larger singular values of the error image represent the error information corresponding to the occlusion, the smaller ones represent normal image pixels. When using the low-rank approximation for the error image, we hope the error image contains the occlusion information as much as possible and face information as less as possible. Thus we should give less punishment to larger singular values and larger punishment to smaller singular values. Then the resulted error image under a low-rank constraint nearly only contains the error information, which means a better approximation. To achieve a better low-rank approximation, some researchers use the non-convex relaxations (Xie et al. 2017; Zheng et al. 2019; Dong, Zheng, and Lian 2019). (Luo et al. 2016) used the Schatten- p -norm and obtained a more accurate estimation for error image. (Xie et al. 2017) proposed to use a set of non-convex function to better approximate the low-rank structure of the error image. However, the Schatten- p -norm treats all the singular value equally, and the convex relaxations in (Luo et al. 2016) may not an optimal of low-rank approximation.

Considering that existing methods mentioned above cannot fit the complex representation error distribution and structure very well, in this paper, we propose a unified sparse weight learning and low-rank approximation regression model based on the generalized correntropy to tackle these problems. By choosing different α values in the generalized correntropy, the proposed model can fit various error distribution and approximate the rank of error very well, which can be seen from Figure 1. The key points of the proposed method are summarized as follows.

- The first attempt to use only one function to address both error distribution and structure estimation.
- The proposed algorithm can better fit the complicated error distribution caused by the variation of illumination, expressions, poses, positions, noise, and occlusions.
- A new and more accurate low-rank approximate estimator is proposed for contiguous error structure estimation.

Related Works

Robust Weight Learning

(He, Zheng, and Hu 2011) proposed a correntropy induced metric (CIM) based loss function for robust face recognition. They adaptively learn a weight for the representation error, by which the larger errors corresponding to the noise and outliers receive smaller weights (larger penalty) while the smaller errors receive larger weights (smaller penalty). Given a query image vector $\mathbf{y} \in R^m$, and the training dataset $\mathbf{D} \in R^{m \times n}$, the CIM-based loss function and weight estimators are defined as follows.

$$\hat{J} = \max_{x, w} \sum_{j=1}^m (w_j (y_j - \sum_{i=1}^n d_{i,j} x_i)^2 - \phi(w_j)) - \lambda \sum_{i=1}^n x_i, \quad \text{subject to (s.t.) } x_i \geq 0, \quad i = 1, \dots, n. \quad (1)$$

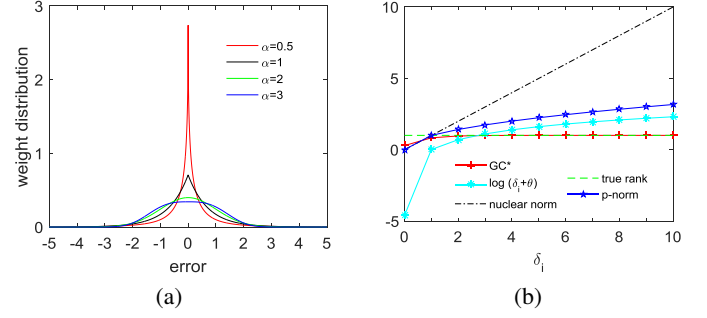


Figure 1: (a) Weight distribution with different parameters; (b) The approximation of different functions for the rank function. Note that the approximated rank of the error by the proposed method (in red) has almost overlapped with the true rank (in green) when δ_i is greater than 2.

where the weight is calculated by

$$w_j^{t+1} = -g(y_j - \sum_{i=1}^n d_{i,j} x_i^t), \quad (2)$$

where $g(x)$ is the Gaussian function. Considering that the Gaussian function in (He, Zheng, and Hu 2011) is not robust enough to match the error when there are heavy noise and large occlusions, (Iliadis et al. 2017) and (Yang et al. 2012) proposed to use the logistic function as a weight descriptor to match the error distribution

$$w_j^{t+1} = \frac{\exp(-\gamma e_i^2 + \gamma \theta)}{1 + \exp(-\beta e_i^2 + \beta \theta)}. \quad (3)$$

Different from learning weight using a specific function as in (He, Zheng, and Hu 2011; Iliadis et al. 2017), (Zheng et al. 2017) proposed an iterative procedure to adaptively learn the weight by solving a constrained sparse learning problem. Their model is defined as follows:

$$\argmin_{\mathbf{w}^T \mathbf{1} = 1, \mathbf{w}} \frac{1}{2} \|\sqrt{\mathbf{w}}(\mathbf{y} - \mathbf{D}\mathbf{x})\|_2^2 + \gamma \|\mathbf{w}\|_2^2, \quad (4)$$

where $\mathbf{w} = [\omega_1, \dots, \omega_j, \dots, \omega_m]$ with each ω_j updated by

$$w_j^{t+1} = (-\frac{\mathbf{d}}{2\gamma} + \eta)_+, \quad (5)$$

where $d_i = e_i^2$, and η is the Lagrangian multiplier. Here $(\cdot)_+$ is a threshold function.

Low-Rank Approximation

Both (Iliadis et al. 2017) and (Yang et al. 2016) introduce the nuclear norm as the low-rank approximation of the error image in the presence of contiguous occlusions. Assume the matrix \mathbf{E} is the error image, they calculate the rank-constrained error using the following formulation.

$$\min_{\hat{\mathbf{E}}} \frac{1}{2} \|\hat{\mathbf{E}} - \mathbf{E}\|_F^2 + \lambda \|\hat{\mathbf{E}}\|_*, \quad (6)$$

where the nuclear norm $\|\cdot\|_*$ is a rank approximation function. Then the optimal low-rank constrained error image is given by

$$\hat{\mathbf{E}}^* = \mathbf{U}\mathbf{S}\mathbf{V}^T, \quad (7)$$

where \mathbf{U} , \mathbf{V} are the left and right singular vectors of \mathbf{E} , $\mathbf{S} = \text{sign}(\delta_i) \max(0, |\delta_i| - \lambda)$, and δ_i is the singular value of \mathbf{E} .

Since the nuclear norm based low-rank approximation treats each singular value equally regardless their contributions to the error image. (Xie et al. 2017) proposed to use the non-convex function to better approximate the low-rank structure of the error image. They use the l_p -norm, log-sum, atan, and log-exp functions as the non-convex relaxation of the rank function. Their robust low-rank model is

$$\min_{\hat{\mathbf{E}}} \frac{1}{2} \|\hat{\mathbf{E}} - \mathbf{E}\|_F^2 + \lambda \|\hat{\mathbf{E}}\|_{\omega,*} \quad (8)$$

which has the following closed-form

$$\hat{\mathbf{E}}^* = \mathbf{U} \mathbf{S}_{\omega,*} \mathbf{V}^T, \quad (9)$$

where \mathbf{U} and \mathbf{V} are the left and right singular vectors of \mathbf{E} , and $\mathbf{S}_{\omega,*}$ is the weighted Singular Value Thresholding (SVT) operator,

$$\mathbf{S}_{\omega,*} = \text{diag}(\max(\delta_i - \omega_i \lambda, 0)), \quad i = 1, 2, \dots, m_2, \quad (10)$$

where δ_i is the singular value of \mathbf{E} , and ω_i is a weight controlling the shrinkage level of each singular value.

Proposed Method

In this section, the generalized correntropy metric (GCM) is proposed for face recognition. The GCM introduces a nonconvex penalty to enhance the sparsity in both the intrinsic low-rank structure and sparse corruption. The proposed GCM penalty can overcome the aforementioned drawbacks of the sparse corruption and nuclear norm.

The GCM Penalty

Inspired by the remarkable performance of nonconvex regularizers used for image processing (Xie et al. 2017), a nonconvex regularizer represented as $f_{GC}(x)$ is introduced to measure the contribution of each point $\mathbf{e} \in R^m$. $f_{GC}(x)$ is defined as the generalized correntropy loss function by

$$\begin{aligned} f_{GC}(A, B) &= \frac{1}{2} E [\|\varphi_{\alpha,\beta}(A) - \varphi_{\alpha,\beta}(B)\|_{\mathcal{H}}^2] \\ &= \frac{1}{2} E [\langle \varphi_{\alpha,\beta}(A), \varphi_{\alpha,\beta}(A) \rangle + \langle \varphi_{\alpha,\beta}(B), \varphi_{\alpha,\beta}(B) \rangle \\ &\quad - 2 \langle \varphi_{\alpha,\beta}(A), \varphi_{\alpha,\beta}(B) \rangle] \\ &= E [G_{\alpha,\beta}(0) - G_{\alpha,\beta}(\mathbf{e})] \end{aligned} \quad (11)$$

where $\mathbf{e} = A - B$, $E(x)$ is the expectation of x , $\varphi_{\alpha,\beta}(\cdot)$ denotes a nonlinear mapping which transforms its argument into a high-dimensional Hilbert space (Chen et al. 2016), and $G_{\alpha,\beta}$ is the Generalized Gaussian Density (GGD) function

$$\begin{aligned} G_{\alpha,\beta}(e) &= \frac{\alpha}{2\beta\Gamma(1/\alpha)} \exp\left(-\left|\frac{e}{\beta}\right|^\alpha\right) \\ &= \gamma_{\alpha,\beta} \exp(-\lambda |e|^\alpha). \end{aligned} \quad (12)$$

Here $\alpha > 0$ and $\beta > 0$ are the parameters of GGD indicating the peak and width of the probability density function. $\Gamma(z) = \int_0^\infty e^{-t} t^{z-1} dt$, ($z > 0$) is the gamma function. $\lambda = 1/\beta^\alpha$ and $\gamma_{\alpha,\beta} = \alpha/(2\beta\Gamma(1/\alpha))$ are the kernel

parameter and the normalization constant, respectively. Obviously, the Gaussian function is just a special case of the generalized Gaussian density function when α is 2. When α is 1, (12) becomes the Laplacian distribution. We plot the GGD distributions with several shape parameters in Figure 1(a) which shows that smaller values of α give heavier tails (sharper distributions). When $\alpha \rightarrow \infty$, the GGD is close to the uniform distribution, while $\alpha \rightarrow 0_+$ approaches an impulse function. Thus, owing to the flexibility of shape parameter selection, the GGD function can match the errors of different distributions very well.

By combining (11) and (12), the generalized correntropy function in (11) can be rewritten as another form as

$$f_{GC}(\mathbf{e}) = \gamma_{\alpha,\beta} (1 - \exp(-\lambda |\mathbf{e}|^\alpha)) \quad (13)$$

which can be used for the weight learning. Here we use the $\|\mathbf{e}\|_\infty$ to normalize the representation error and ensure the errors to be in the same scale, i.e. $\mathbf{e} = \frac{\mathbf{e}}{\|\mathbf{e}\|_\infty}$. For the low-rank approximation, the GC-function is defined as follows:

$$f_{GC}(\delta(\mathbf{E})) = \gamma_{\alpha,\beta} (1 - \exp(-\lambda |\delta(\mathbf{E})|^\alpha)) \quad (14)$$

where \mathbf{E} is the matrix form of the representation error vector \mathbf{e} , and $\delta(\mathbf{E})$ represents the singular values of \mathbf{E} .

We can see that the function $f_{GC}(\bullet)$ treats each entry adaptively. For the weight learning, it gives a larger weight for a smaller error, while gives a smaller weight for a larger error, which reduces the influence of outliers. For the low-rank constraint, it shrinks the larger singular value less and the smaller value more, which can better approximate the rank of the error image. Figure 1 shows the error fitting curve and the rank approximation using different functions. In Figure 1(a), the GC function can fit different levels of error, especially the smaller residual errors. Figure 1(b) shows that the GC-function has a good approximation of the true rank.

The Proposed GCM

Motivated by the advantages of the GC-function in learning discriminative weights and in approximating rank for representation errors, we consider to use $f(\mathbf{e})$ and $f(\sigma(\mathbf{E}))$ as the vector weight and matrix rank surrogate function to learn more robust features for face recognition in the presence of noise, outliers, and occlusions. The proposed GCM model for robust face recognition is defined as

$$\begin{aligned} \min_{\mathbf{w}, \mathbf{x}} f_{GC}(\mathbf{e}) + \lambda_1 f_{GC}(\sigma(\mathbf{E})) + \lambda_2 v(\mathbf{x}), \\ \text{s.t. } \mathbf{y} - \mathbf{D}\mathbf{x} = \mathbf{e}, \quad \mathbf{E} = T\mathbf{M}(\mathbf{e}). \end{aligned} \quad (15)$$

where $\lambda_1 > 0$ and $\lambda_2 > 0$ are regularization parameters used to control the tradeoff between the constraints of sparsity and matrix rank, and $T\mathbf{M}(\mathbf{x})$ means transforming the vector \mathbf{x} to the matrix form \mathbf{X} .

Optimization by Majorization Minimization

In this section, we use a majorization minimization (MM) algorithm to solve problem (15). In MM, instead of solving the complicated nonconvex optimization problem directly, it replaces the original function with its upper bound surrogate function in majorization step and then minimize the resulted function in minimization step.

Majorization Procedure

We first find the majorization function (upper bound) $f(\mathbf{x}|\mathbf{x}^t)$ of $f(\mathbf{x})$, which satisfies $f(\mathbf{x}|\mathbf{x}^t) \geq f(\mathbf{x})$. Then the optimal solution to the surrogate function can be solved by

$$\mathbf{x}_{t+1} = \underset{\mathbf{x}}{\operatorname{argmin}} f(\mathbf{x}|\mathbf{x}_t). \quad (16)$$

As in (Sun, Babu, and Palomar 2016), the first order Taylor expansion of $f(\mathbf{x})$ is used as a surrogate function as follows:

$$f(\mathbf{x}) \leq f(\mathbf{x}_t) + f'(\mathbf{x}_t)(\mathbf{x} - \mathbf{x}_t) = f(\mathbf{x}|\mathbf{x}_t). \quad (17)$$

Then $f(\mathbf{x})$ can be upperbounded as

$$f(\mathbf{x}) \leq f(\mathbf{x}_t) + f'(\mathbf{x}_t)\mathbf{x} + c, \quad (18)$$

where c is a constant. Thus, the majorization functions for the weight learning and low-rank approximation are

$$f_{GC}(\mathbf{e}) \leq f_{GC}(\mathbf{e}_t) + f'_{GC}(\mathbf{e}_t)(\mathbf{e} - \mathbf{e}_t), \quad (19)$$

and

$$f_{GC}(\delta(\mathbf{E})) \leq f_{GC}(\delta_t(\mathbf{E})) + f'_{GC}(\delta_t(\mathbf{E}))(\delta(\mathbf{E}) - \delta_t(\mathbf{E})). \quad (20)$$

$f(\mathbf{e})$ can be upper bounded as

$$f_{GC}(\mathbf{e}) \leq f_{GC}(\mathbf{e}_t) + f'_{GC}(\mathbf{e}_t)\mathbf{e} + c = f_{GC}(\mathbf{e}|\mathbf{e}_t), \quad (21)$$

and $f(\delta(\mathbf{E}))$ as

$$\begin{aligned} f_{GC}(\delta(\mathbf{E})) &\leq f_{GC}(\delta_t(\mathbf{E})) + f'_{GC}(\delta_t(\mathbf{E}))\delta(\mathbf{E}) + c \\ &= f_{GC}(\delta(\mathbf{E}|\delta_t(\mathbf{E}))). \end{aligned} \quad (22)$$

Minimization Procedure

Based on the above analysis, minimizing the objective function in (15) can be solved by minimizing the following surrogate function

$$\begin{aligned} \underset{\mathbf{e}, \mathbf{x}, \mathbf{h}}{\operatorname{argmin}} \quad & f_{GC}(\mathbf{e}|\mathbf{e}_t) + \lambda_1 f_{GC}(\sigma(\mathbf{E})|\sigma_t(\mathbf{E})) + \lambda_2 v(\mathbf{h}), \\ \text{s.t.} \quad & \mathbf{y} - \mathbf{D}\mathbf{x} = \mathbf{e}, \quad \mathbf{E} = TM(\mathbf{e}), \quad \mathbf{x} = \mathbf{h}. \end{aligned} \quad (23)$$

The Lagrangian function of (23) is

$$\begin{aligned} \mathcal{L}(\mathbf{e}, \mathbf{x}, \mathbf{h}, \mathbf{v}_1, \mathbf{v}_2) &= f_{GC}(\mathbf{e}|\mathbf{e}_t) + \lambda_1 f_{GC}(\sigma(\mathbf{E})|\sigma_t(\mathbf{E})) \\ &+ \lambda_2 v(\mathbf{h}) + \mathbf{v}_1^T (\mathbf{y} - \mathbf{D}\mathbf{x} - \mathbf{e}) + \frac{\rho_1}{2} \|\mathbf{y} - \mathbf{D}\mathbf{x} - \mathbf{e}\|_2^2 \\ &+ \mathbf{v}_2^T (\mathbf{x} - \mathbf{h}) + \frac{\rho_2}{2} \|\mathbf{x} - \mathbf{h}\|_2^2, \end{aligned} \quad (24)$$

where ρ_1 and ρ_2 are positive penalty parameters, and \mathbf{v}_1 and \mathbf{v}_2 are the dual variables. The optimal parameters can be updated by the following ADMM procedure.

$$\begin{aligned} \mathbf{e}_{t+1} &= \underset{\mathbf{e}}{\operatorname{argmin}} \mathcal{L}(\mathbf{e}, \mathbf{x}_t, \mathbf{h}_t, \mathbf{v}_{1,t}, \mathbf{v}_{2,t}), \\ \mathbf{h}_{t+1} &= \underset{\mathbf{z}}{\operatorname{argmin}} \mathcal{L}(\mathbf{e}_{t+1}, \mathbf{x}_t, \mathbf{h}, \mathbf{v}_{1,t}, \mathbf{v}_{2,t}), \\ \mathbf{x}_{t+1} &= \underset{\mathbf{x}}{\operatorname{argmin}} \mathcal{L}(\mathbf{e}_{t+1}, \mathbf{x}, \mathbf{h}_{t+1}, \mathbf{v}_{1,t}, \mathbf{v}_{2,t}), \\ \mathbf{v}_{1,t+1} &= \mathbf{v}_{1,t} + \rho_1 (\mathbf{y} - \mathbf{D}\mathbf{x}_{t+1} - \mathbf{e}_{t+1}), \\ \mathbf{v}_{2,t+1} &= \mathbf{v}_{2,t} + \rho_2 (\mathbf{x}_{t+1} - \mathbf{h}_{t+1}). \end{aligned} \quad (25)$$

• **Updating \mathbf{e}_{t+1} :** the optimal \mathbf{e}_{t+1} can be updated by the following problem,

$$\begin{aligned} \mathbf{e}_{t+1} &= \underset{\mathbf{e}}{\operatorname{argmin}} f_{GC}(\mathbf{e}|\mathbf{e}^t) + \lambda_1 f_{GC}(\sigma(\mathbf{E})|\sigma^t(\mathbf{E})) \\ &+ \mathbf{v}_1^T (\mathbf{y} - \mathbf{D}\mathbf{x} - \mathbf{e}) + \frac{\rho_1}{2} \|\mathbf{y} - \mathbf{D}\mathbf{x} - \mathbf{e}\|_2^2. \end{aligned} \quad (26)$$

To calculate \mathbf{e}_{t+1} , we consider a two-step fast approximation. In Step one, we first solve the following problem.

$$\begin{aligned} \hat{\mathbf{e}} &= \underset{\mathbf{e}}{\operatorname{argmin}} f_{GC}(\mathbf{e}|\mathbf{e}^t) + \mathbf{v}_1^T (\mathbf{y} - \mathbf{D}\mathbf{x} - \mathbf{e}) \\ &+ \frac{\rho_1}{2} \|\mathbf{y} - \mathbf{D}\mathbf{x} - \mathbf{e}\|_2^2. \end{aligned} \quad (27)$$

where

$$\begin{aligned} f_{GC}(\mathbf{e}|\mathbf{e}_t) &= f'_{GC}(\mathbf{e}|\mathbf{e}_t)\mathbf{e} \\ &= [\gamma_{\alpha, \beta}(1 - \exp(-\lambda|\mathbf{e}_t|^\alpha))]'\mathbf{e} \\ &= [\gamma_{\alpha, \beta}(1 - \exp(-\lambda|\mathbf{e}_t^2|^{\frac{\alpha}{2}}))]'\mathbf{e}^2 \\ &= \frac{1}{2}\gamma_{\alpha, \beta}\lambda\alpha\exp(-\lambda|\mathbf{e}_t^2|^{\frac{\alpha}{2}})|\mathbf{e}_t|^{\frac{\alpha}{2}-1}\mathbf{e}^2 \\ &\propto \|\sqrt{\mathbf{w}} \odot \mathbf{e}\|_2^2 \end{aligned} \quad (28)$$

where $\mathbf{w} = \exp(-\lambda\|\mathbf{e}_t^2\|^{\frac{\alpha}{2}})|\mathbf{e}_t|^{\frac{\alpha}{2}-1}$. Thus (27) can be rewritten as

$$\begin{aligned} \hat{\mathbf{e}} &= \underset{\mathbf{e}}{\operatorname{argmin}} \|\sqrt{\mathbf{w}} \odot \mathbf{e}\|_2^2 + \mathbf{v}_1^T (\mathbf{y} - \mathbf{D}\mathbf{x} - \mathbf{e}) \\ &+ \frac{\rho_1}{2} \|\mathbf{y} - \mathbf{D}\mathbf{x} - \mathbf{e}\|_2^2. \\ &= \left\| \begin{bmatrix} \sqrt{\frac{\rho_1}{2}}(\mathbf{y} - \mathbf{D}\mathbf{x} + \frac{\mathbf{v}_1}{\rho_1}) \\ \mathbf{0} \end{bmatrix} - \begin{bmatrix} \sqrt{\frac{\rho_1}{2}} \\ -\sqrt{\mathbf{w}} \end{bmatrix} \mathbf{e} \right\|_2^2. \end{aligned} \quad (29)$$

Obviously, (29) has a closed-form solution, i.e.,

$$\hat{\mathbf{e}} = \frac{\mathbf{y} - \mathbf{D}\mathbf{x} + \frac{\mathbf{v}_1}{\rho_1}}{\mathbf{I} + \frac{2\mathbf{w}}{\rho_1}}. \quad (30)$$

We then solve the low-rank approximation problem in Step two as follows.

$$\begin{aligned} \mathbf{E}_{t+1} &= \underset{\mathbf{E}}{\operatorname{argmin}} \frac{1}{2} \|\mathbf{E} - \hat{\mathbf{E}}\|_F^2 + \lambda_1 f_{GC}(\delta(\mathbf{E})|\delta^t(\mathbf{E})) \\ &= \underset{\mathbf{E}}{\operatorname{argmin}} \frac{1}{2} \|\mathbf{E} - \hat{\mathbf{E}}\|_F^2 + \lambda_1 \sum_{i=1}^m f'_{GC}(\delta_i(\mathbf{E}))\delta_i \\ &= \underset{\mathbf{E}}{\operatorname{argmin}} \frac{1}{2} \|\mathbf{E} - \hat{\mathbf{E}}\|_F^2 + \lambda_1 \|\mathbf{E}\|_{GC^*} \end{aligned} \quad (31)$$

where $\|\mathbf{E}\|_{GC^*}$ is the proposed robust low-rank approximation. \mathbf{E} can be updated by $\mathbf{E} = \mathbf{U}\mathbf{\Sigma}\mathbf{V}^T$, where $\mathbf{\Sigma} = \operatorname{diag}(a_1, \dots, a_m)$ with $a_i = \max(\delta_i - w_i\lambda_1, 0)$. $\mathbf{U}\operatorname{diag}(\delta_1, \dots, \delta_m)\mathbf{V}^T$ is the singular value decomposition (SVD) of $\hat{\mathbf{E}}$, and $w_i = g'(\delta_i(\mathbf{E}))$. Then the optimal \mathbf{e}_{t+1} is obtained by vectorizing \mathbf{E} .

• **Updating \mathbf{h}_{t+1} :** In this paper, we use the l_2 -norm to regularize the coefficient \mathbf{x} (or \mathbf{h}). We update \mathbf{h}_{t+1} by solving the following problem.

$$\begin{aligned} \mathbf{h}_{t+1} &= \underset{\mathbf{h}}{\operatorname{argmin}} \lambda_2 \|\mathbf{h}\|_2^2 + \frac{\rho_1}{2} \|\mathbf{x}_t - \mathbf{h}\|_2^2 + \mathbf{v}_2^T (\mathbf{x} - \mathbf{h}) \\ &= (\mathbf{x}_t + \frac{\mathbf{v}_2}{\rho_2})_+. \end{aligned} \quad (32)$$

• **Updating \mathbf{x}_{t+1}**

$$\begin{aligned} \mathbf{x}_{t+1} = \underset{\mathbf{x}}{\operatorname{argmin}} \frac{\rho_1}{2} \|\mathbf{y} - \mathbf{D}\mathbf{x} - \mathbf{e}_{t+1}\|_2^2 + \mathbf{v}_{1,t}^T (\mathbf{y} - \mathbf{D}\mathbf{x} - \mathbf{e}_{t+1}) \\ + \mathbf{v}_{2,t}^T (\mathbf{x} - \mathbf{h}_{t+1}) + \frac{\rho_2}{2} \|\mathbf{x} - \mathbf{h}_{t+1}\|_2^2. \end{aligned} \quad (33)$$

The optimal \mathbf{x}_{t+1} can be obtained by solving the following closed-form problem

$$\left\| \begin{bmatrix} \sqrt{\frac{\rho_1}{2}} (\mathbf{y} - \mathbf{e}_{t+1} + \frac{\mathbf{v}_{1,t}}{\rho_1}) \\ \sqrt{\frac{\rho_2}{2}} (\mathbf{h}_{t+1} - \frac{\mathbf{v}_{2,t}}{\rho_2}) \end{bmatrix} - \begin{bmatrix} \sqrt{\frac{\rho_1}{2}} \mathbf{D} \\ \sqrt{\frac{\rho_2}{2}} \mathbf{I} \end{bmatrix} \mathbf{x} \right\|_2^2. \quad (34)$$

Thus, the optimal \mathbf{x}_{t+1} is given by

$$\mathbf{x}_{t+1} = \frac{\rho_1 \mathbf{D}^T (\mathbf{y} - \mathbf{e}_{t+1} + \frac{\mathbf{v}_{1,t}}{\rho_1}) + \rho_2 (\mathbf{h}_{t+1} - \frac{\mathbf{v}_{2,t}}{\rho_2})}{\rho_1 \mathbf{D}^T \mathbf{D} + \rho_2 \mathbf{I}}. \quad (35)$$

The unified weight learning and low-rank approximation (UWLLA) algorithm is summarized in Algorithm 1.

Algorithm 1 The UWLLA Algorithm

Input: Given a test image $\mathbf{y} \in R^m$, and a set of training images $\mathbf{D} = [\mathbf{d}_1, \mathbf{d}_2, \dots, \mathbf{d}_n] \in R^{m \times n}$ with each $\mathbf{d}_i \in R^m$ being a training sample, $\alpha, \beta, \lambda_1, \lambda_2, \rho_1$ and ρ_2 . Initializing \mathbf{e} with \mathbf{y} .

Output: $\mathbf{x}^*, \mathbf{w}^*$.

```

1: while  $t=1, \dots, T$  do
2:   Updating weights by
3:    $\mathbf{w} = \exp(-\lambda \|\mathbf{e}_t\|_2^{\frac{\alpha}{2}}) \|\mathbf{e}_t\|_2^{\frac{\alpha}{2}-1}$ .
4:   Updating  $\hat{\mathbf{e}}$  by (27)-(30).
5:   Updating  $\mathbf{E}_{t+1}$  by (31).
6:   Updating  $\mathbf{h}_{t+1}$  by (32).
7:   Updating  $\mathbf{x}_{t+1}$  by (35).
8:   Updating  $\mathbf{v}_{1,t+1}$  by  $\mathbf{v}_{1,t+1} = \mathbf{v}_{1,t} + \rho_1 (\mathbf{y} - \mathbf{D}\mathbf{x} - \mathbf{e})$ .
9:   Updating  $\mathbf{v}_{2,t+1}$  by  $\mathbf{v}_{2,t+1} = \mathbf{v}_{2,t} + \rho_2 (\mathbf{x}_{t+1} - \mathbf{h}_{t+1})$ .
10:  if  $\epsilon > 1e-5$  then
11:    repeat;
12:  else
13:     $t \leftarrow t + 1$ ; Break;
14:  end if
15: end while
16: Identity  $(\mathbf{y}) = \operatorname{argmin}_i \|\sqrt{\mathbf{w}^*} (\mathbf{y} - \mathbf{D} \mathbf{k}_i(\mathbf{x}^*))\|_2^2$ , where  $\mathbf{k}_i(\mathbf{x}^*)$  is a subvector of  $\mathbf{x}^*$  corresponding to the coefficients of training samples from the  $i$ -th class.

```

Computational Complexity and Convergence

Suppose $\mathbf{y} \in R^m$ and $\mathbf{Y} \in R^{m_1 \times m_2} (m_1 \leq m_2)$ are a testing image vector and its matrix form, and the training set is $\mathbf{D} \in R^{m \times n}$. The computational complexity for Step 3 in Algorithm 1 is $O(n)$, for Step 4 is $O(mn)$ which is determined by the matrix multiplication $\mathbf{D}\mathbf{x}$, and for Step 5 is $O(m_1 m_2^2)$ which is determined by the SVD of matrix \mathbf{E} . Step 7 requires mn multiplications for $\mathbf{D}^T \mathbf{y}$. Thus, the total computational complexity for Algorithm 1 is $O(T(n + mn + m_1 m_2^2 + mn))$, where T is the number of iterations.

The convergence analysis of MM has been well studied in (Hunter and Lange 2004), thus according to the theory of MM, we have $f_{\text{GC}}(\mathbf{e}_{t+1}) \leq f_{\text{GC}}(\mathbf{e}_t)$, and $f_{\text{GC}}(\delta(\mathbf{E})_{t+1}) \leq f_{\text{GC}}(\delta(\mathbf{E})_t)$, which indicates that the objective function in (15) will monotonically decrease. Moreover, the ADMM optimization problem in the UWLLA algorithm can be divided into three main subproblems (refer to (25)), each of which is convex with respect to one variable. The convergence analysis of the ADMM algorithm has been well studied in (Boyd et al. 2011; Yang et al. 2016; Shang et al. 2017), and has been further verified in different applications, such as (Hu and Chen 2018; Zhu et al. 2017; Piao et al. 2019). Thus, we can find a locally optimal solution for each subproblem.

Experimental results

Databases and Parameter Settings

To verify the effectiveness of the proposed algorithm, we carry out experiments on three public face databases, including Extended Yale B (ExYaleB) (A.S. Georghiades and Kriegman 2001), AR (Martinez and Benavente 1998), and aligned Labeled Face in the wild (LFW-a) (Wolf, Hassner, and Taigman 2009). The proposed algorithm is tested and compared with recently published face recognition approaches, including CESR (He, Zheng, and Hu 2011), RRC-L1 and RRC-L2 (Yang et al. 2012), HQ-A and HQ-M (He et al. 2013), F-LR-IRNNLS (Iliadis et al. 2017), IRGSC (Zheng et al. 2017), NMR (Yang et al. 2016).

α and β are two important parameters in the proposed regression model where the former models the shape of the error distribution, and the latter is the kernel width. Denoted by α_1 and β_1 the parameters for the weight learning, and α_2 and β_2 for the rank approximation. In this paper, $1 < \alpha_1 < 2$ is used for weight learning for all the experiments. We fixed $\alpha_2 = 1$ and $\beta_2 = 0.7$ for a better low-rank approximation for all the experiments. For the proposed ADMM optimization algorithm, we use $\rho_1 = 1, \rho_2 = 0.1, \lambda_1 = 0.01, \lambda_2 = 1$.

Experiments on the ExYaleB database

In this experiment, the images from the ExYaleB face database are resized to 96×84 pixels. We adopt two experimental settings, one is the testing data with different percentages of occlusions, another is the testing data with different levels of occlusion-pixel mixed corruptions. For both experiments, we choose all the images in subsets 1 and 2 for training, and subset 3 for testing. Thus, the total number of images for training and testing are 719 and 455, respectively.

In the first experiment, we evaluate the proposed algorithm on the dataset with occlusion percentage varying from 20% to 70%. To simulate occlusions, we randomly selected local region in each testing image and replace this area with an unrelated image. In this experiment, we use the baboon image, as used in (Iliadis et al. 2017; Xie et al. 2017), for occlusion. To simulate a specific percentage of occlusion for a testing image $\mathbf{Y} \in R^{m_1 \times m_2}$, we resize the baboon image to $z \times z$, where $z = \sqrt{m_1 \times m_2 \times x\%}$ and replace the local region in the testing image. One example of the occluded test-

Table 1: The recognition accuracy of all the algorithms on the ExYaleB face database with 60% occlusion (60% Occ.) and 60% mixed corruption (60% Mix.).

Corruptions	Methods								
	CESR	RRC-L1	RRC-L2	HQ-A	HQ-M	FLR-IRNNLS	IRGSC	NMR	Proposed
60% Occ.	41.85	69.67	70.54	48.02	68.13	95.82	66.15	79.12	98.46
60% Mix.	27.27	34.72	35.60	17.92	32.15	49.01	27.91	8.64	64.75

ing image is show in Figure 2 (b). The recognition accuracy of all algorithms on the data with 60% occlusion are shown in Table 1 where the proposed algorithm obtained the highest accuracy 98.46%. The recognition rates from the proposed method and all the benchmarks under different percent of occlusions are shown in Figure 3(a), which show that our method nearly 100% recognize testing images when occlusion percent is no larger than 50%, and still maintain the highest accuracy when occlusion percent is larger than 50%. Especially, the accuracy of the proposed method are nearly 3% and 30% higher than that of the second largest one under case of 60% and 70% occlusion, respectively.



Figure 2: Face images of the ExYaleB database with different types of corruptions. (a) A clean face image. (b) with 30% percent of block occlusion. (c) with 30% occlusion-pixel mixed corruption. Here 30% mixed noise means 30% random pixel corruptions plus 30% occlusions.

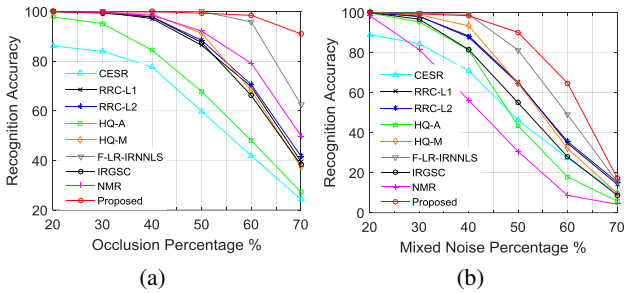


Figure 3: Recognition accuracies with different types of corruptions on the ExYaleB database. (a) with different percentage of occlusions. (b) with mixed corruptions.

To evaluate the performance of the proposed method under more challenging conditions, we test it on the dataset with different levels of mixed pixel corruptions and block occlusions. The corruption level varies from 20% to 70%. To simulated the mixed corruptions, we randomly select a certain percent of pixels and replace them with random values, an example image with 30% percent of mixed corruptions is shown in Figure 2(c). The recognition accuracy of all the

algorithms with 60% mixed corruptions are shown in Table 1 where the proposed algorithm obtains the best accuracy. The accuracies of all the algorithms with varying levels of corruptions are shown in Figure 3(b) which shows that the proposed algorithm can tolerate the mixed corruptions very well, and is superior to other benchmarks.

Experiments on the AR database

In this experiment, we also test the proposed algorithm on the dataset with real sunglasses and scarf occlusions, and mixed corruptions. In AR database, there are two sessions of facial images from 100 subjects (50 male and 50 female). In each session, there are 2 natural unoccluded face images, 3 face images with scarf disguise and 3 with sunglasses. Some examples of the testing image are shown in Figure 4.

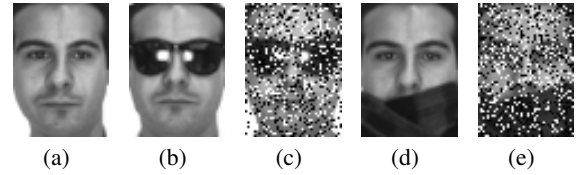


Figure 4: Face images of the AR database with different corruptions. (a) A clean face image. (b) with sunglass occlusion. (c) with sunglass-pixel corruption. (d) with scarf occlusion. (e) with scarf-pixel corruption.

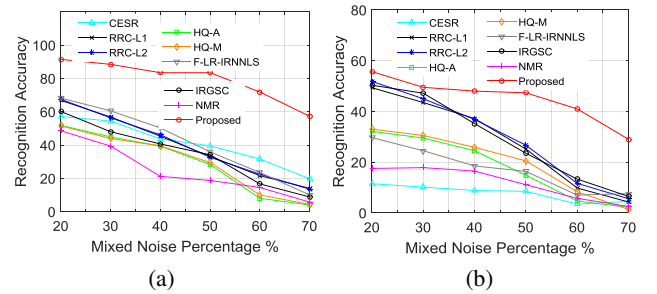


Figure 5: Recognition accuracies under different types of corruptions on the AR database. (a) under different percentages of sunglasses-random pixel corruptions; (b) under different percentages scarf-random pixel mixed corruptions.

We first test the proposed algorithm on session 1 and 2 separately. For both sessions, we select the only natural unoccluded image as the training image, and 3 images with sunglasses and 3 images with scarf for testing. Then, we test the proposed algorithm on the data from both sessions, here

Table 2: The recognition accuracy of all the algorithms on the AR face database with different occlusions.

Evaluation Types		Methods								
		CESR	RRC-L1	RRC-L2	HQ-A	HQ-M	FLR-IRNNLS	IRGSC	NMR	Proposed
Session 1	sunglass	60.54	75.33	77.00	68.00	72.67	83.33	73.33	75.67	93.00
	scarf	19.46	61.66	64.33	30.54	35.23	55.67	54.33	60.74	66.33
Session 2	sunglass	67.11	82.66	83.66	70.13	72.48	86.24	77.67	80.47	93.67
	scarf	13.67	60.66	61.66	25.33	30.00	48.00	54.33	54.00	63.00
Both sessions	sunglass	66.72	83.00	83.16	70.23	72.58	85.79	77.33	72.53	94.67
	scarf	17.33	67.33	69.33	29.67	34.17	57.33	62.83	64.00	71.33

2 natural images are selected as training images, and 6 images with sunglasses and 6 images with scarf for testing. The recognition rates from the proposed algorithm and all the benchmarks are shown in Table 2, which shows that the proposed algorithm outperforms all the benchmarks in terms of single session and both session testing. Figure 5 displays the performance of all the algorithms with different levels of sunglasses-random pixel mixed and scarf-random pixel mixed corruptions. The accuracy curves show that the proposed algorithm significantly outperforms the benchmarks.

Experiments on the LFW database

To evaluate the robustness of the proposed algorithm for face recognition under an unconstrained environment, we then carry out experiments on the LFW database. We use the aligned version LFW-a database for all the experiments. We select 158 subjects with each subject no less than 10 samples. For each subject, we randomly select 5 samples for training and 5 samples for testing. Thus, the number of training samples and testing samples are both 790.

First, we test all the algorithms on the clean image to verify the effectiveness of the proposed algorithm in fitting the representation error caused by illumination, pose, and expression changes. Two types of corruptions, i.e. block occlusion (baboon image) and occlusion-pixel mixed corruption, are adopted to further evaluate the robustness of the proposed algorithm. All the algorithms are tested on the data with 20% block occlusion (20% Occ.), 20% mixed corruptions (20% Mix.), 40% Occ., and 40% Mix.. Table 3 lists the recognition accuracy of different algorithms on the clean and corrupted datasets, which shows that the proposed algorithm is superior to other benchmarks in a complex environment.

Discussion on the selection of α and β

According to above experimental results, we empirically choose values of α_1 and β_1 from $\alpha_1 \in [1, 2]$ and $\beta_1 \in [0.05, 0.15]$ for the robust weight learning. When the errors are disturbed by larger outliers which will cause heavy-tailed noise, then a lower-order statistical measure (smaller α_1) for the error is usually more robust. In this paper, we use $\alpha_1 = 1.7$ for all the experiments to handle different types of corruptions. Choosing the value of β_1 is also important for the proposed model. A smaller β_1 leads to a thinner distribution, while larger β_1 leads to a fatter distribution. The error with a thinner distribution is usually caused by a simple corruption, e.g., corruption from different occlusions. A fatter

Table 3: The recognition accuracy of all the algorithms on the clean LFW database and data with various corruptions.

Methods	Different types /percentages of corruptions				
	Clean	20% Occ.	20% Mix.	40% Occ.	40% Mix.
CESR	59.95	54.75	50.19	35.28	23.35
RRC-L1	68.98	65.06	63.29	47.34	25.56
RRC-L2	69.36	60.12	57.08	40.63	19.62
HQ-A	51.27	51.33	57.09	35.28	30.33
HQ-M	58.30	58.63	58.94	43.91	32.99
FLR-IRNNLS	71.65	63.37	62.74	51.02	37.56
IRGSC	73.42	65.33	50.51	37.09	13.04
NMR	72.62	54.63	41.83	32.23	14.45
Proposed	74.18	66.78	65.19	52.03	46.70

distribution is caused by more complicated corruptions, e.g., occlusion-pixel mixed corruptions. Thus, for all the experiments, we use a smaller $\beta_1 = 0.07$ for the experiments with occlusions, and a larger $\beta_1 = 0.11$ for the experiments with occlusion-pixel mixed corruptions. Different from matching the error distribution in weight learning, the GC function for low-rank approximation tries to give more emphasis on the larger singular values and thus can maintain the low-rank structure of the error image. In all the experiments, $\alpha_2 = 1$ and $\beta_2 = 0.7$ can provide a good low-rank approximation.

Conclusions

In this paper, in order to better fit the representation errors caused by various corruptions in face recognition, we proposed a unified sparse weight learning and low-rank regression model based on the generalized correntropy. The sparse weight learning procedure can discriminately weight errors caused by random noises, while the low-rank step can provide a more accurate approximation for structured errors, thus the learned features for the classification are more robust to various corruptions. Moreover, different from existing algorithms in handling both problems with multiple functions, we unify the two targets in one function, which provides a deep investigation of the relationship between sparse weight learning and low-rank approximation. The experimental results show that the proposed algorithm can both handle the complex pixel corruptions as well as the block occlusions.

References

- [A.S. Georgiades and Kriegman 2001] A.S. Georgiades, P. B., and Kriegman, D. 2001. From few to many: Illumination cone models for face recognition under variable lighting and pose. *IEEE Transactions on Pattern Analysis and Machine Intelligence* 23(6):643–660.
- [Boyd et al. 2011] Boyd, S.; Parikh, N.; Chu, E.; Peleato, B.; Eckstein, J.; et al. 2011. Distributed optimization and statistical learning via the alternating direction method of multipliers. *Foundations and Trends® in Machine learning* 3(1):1–122.
- [Chen et al. 2016] Chen, B.; Xing, L.; Zhao, H.; Zheng, N.; and Principe, J. C. 2016. Generalized correntropy for robust adaptive filtering. *IEEE Transactions on Signal Processing* 64(13):3376–3387.
- [Deng, Hu, and Guo 2017] Deng, W.; Hu, J.; and Guo, J. 2017. Face recognition via collaborative representation: Its discriminant nature and superposed representation. *IEEE Transactions on Pattern Analysis And Machine Intelligence* 40(10):2513–2521.
- [Dong, Zheng, and Lian 2019] Dong, J.; Zheng, H.; and Lian, L. 2019. Low-rank laplacian-uniform mixed model for robust face recognition. In *Proceedings of the IEEE Conference on Computer Vision and Pattern Recognition*, 11897–11906.
- [He et al. 2013] He, R.; Zheng, W.-S.; Tan, T.; and Sun, Z. 2013. Half-quadratic-based iterative minimization for robust sparse representation. *IEEE Transactions on Pattern Analysis and Machine Intelligence* 36(2):261–275.
- [He, Zheng, and Hu 2011] He, R.; Zheng, W.-S.; and Hu, B.-G. 2011. Maximum correntropy criterion for robust face recognition. *IEEE Transactions on Pattern Analysis And Machine Intelligence* 33(8):1561–1576.
- [Hu and Chen 2018] Hu, M., and Chen, S. 2018. Doubly aligned incomplete multi-view clustering. In *Twenty-Seventh International Joint Conference on Artificial Intelligence*.
- [Huang et al. 2013] Huang, J.; Nie, F.; Huang, H.; and Ding, C. 2013. Supervised and projected sparse coding for image classification. In *Twenty-Seventh AAAI Conference on Artificial Intelligence*.
- [Hunter and Lange 2004] Hunter, D. R., and Lange, K. 2004. A tutorial on mm algorithms. *The American Statistician* 58(1):30–37.
- [Iliadis et al. 2017] Iliadis, M.; Wang, H.; Molina, R.; and Katsaggelos, A. K. 2017. Robust and low-rank representation for fast face identification with occlusions. *IEEE Transactions on Image Processing* 26(5):2203–2218.
- [Luo et al. 2016] Luo, L.; Yang, J.; Qian, J.; Tai, Y.; and Lu, G.-F. 2016. Robust image regression based on the extended matrix variate power exponential distribution of dependent noise. *IEEE Transactions on Neural Networks and Learning Systems* 28(9):2168–2182.
- [Martinez and Benavente 1998] Martinez, A., and Benavente, R. 1998. The AR face database. Technical report.
- [Naseem, Togneri, and Bennamoun 2012] Naseem, I.; Togneri, R.; and Bennamoun, M. 2012. Robust regression for face recognition. *Pattern Recognition* 45(1):104–118.
- [Piao et al. 2019] Piao, X.; Hu, Y.; Gao, J.; Sun, Y.; and Yin, B. 2019. Double nuclear norm based low rank representation on grassmann manifolds for clustering. In *Proceedings of the IEEE Conference on Computer Vision and Pattern Recognition*, 12075–12084.
- [Qian et al. 2015] Qian, J.; Luo, L.; Yang, J.; Zhang, F.; and Lin, Z. 2015. Robust nuclear norm regularized regression for face recognition with occlusion. *Pattern Recognition* 48(10):3145–3159.
- [Shang et al. 2017] Shang, F.; Cheng, J.; Liu, Y.; Luo, Z.-Q.; and Lin, Z. 2017. Bilinear factor matrix norm minimization for robust pca: Algorithms and applications. *IEEE Transactions on Pattern Analysis and Machine intelligence* 40(9):2066–2080.
- [Sun, Babu, and Palomar 2016] Sun, Y.; Babu, P.; and Palomar, D. P. 2016. Majorization-minimization algorithms in signal processing, communications, and machine learning. *IEEE Transactions on Signal Processing* 65(3):794–816.
- [Wang, Tang, and Li 2016] Wang, Y.; Tang, Y. Y.; and Li, L. 2016. Correntropy matching pursuit with application to robust digit and face recognition. *IEEE Transactions on Cybernetics* 47(6):1354–1366.
- [Wolf, Hassner, and Taigman 2009] Wolf, L.; Hassner, T.; and Taigman, Y. 2009. Similarity scores based on background samples. In *Asian Conference on Computer Vision*, 88–97. Springer.
- [Wright et al. 2009] Wright, J.; Yang, A. Y.; Ganesh, A.; Satri, S. S.; and Ma, Y. 2009. Robust face recognition via sparse representation. *IEEE Transactions on Pattern Analysis And Machine Intelligence* 31(2):210–227.
- [Xie et al. 2017] Xie, J.; Yang, J.; Qian, J. J.; Tai, Y.; and Zhang, H. M. 2017. Robust nuclear norm-based matrix regression with applications to robust face recognition. *IEEE Transactions on Image Processing* 26(5):2286–2295.
- [Yang et al. 2012] Yang, M.; Zhang, L.; Yang, J.; and Zhang, D. 2012. Regularized robust coding for face recognition. *IEEE Transactions on Image Processing* 22(5):1753–1766.
- [Yang et al. 2016] Yang, J.; Luo, L.; Qian, J.; Tai, Y.; Zhang, F.; and Xu, Y. 2016. Nuclear norm based matrix regression with applications to face recognition with occlusion and illumination changes. *IEEE Transactions on Pattern Analysis and Machine Intelligence* 39(1):156–171.
- [Zheng et al. 2017] Zheng, J.; Yang, P.; Chen, S.; Shen, G.; and Wang, W. 2017. Iterative re-constrained group sparse face recognition with adaptive weights learning. *IEEE Transactions on Image Processing* 26(5):2408–2423.
- [Zheng et al. 2019] Zheng, J.; Lou, K.; Yang, X.; Bai, C.; and Tang, J. 2019. Weighted mixed-norm regularized regression for robust face identification. *IEEE Transactions on Neural Networks and Learning Systems*.
- [Zhu et al. 2017] Zhu, X.; Jing, X.-Y.; Wu, F.; Wu, D.; Cheng, L.; Li, S.; and Hu, R. 2017. Multi-kernel low-rank dictionary pair learning for multiple features based image

classification. In *Thirty-First AAAI Conference on Artificial Intelligence*.